

Identification of a Low-Complexity Flow Field Model for AUV Applications

Jan Petrich¹ Craig A. Woolsey² Daniel J. Stilwell¹

¹ The Bradley Department of Electrical and Computer Engineering,

² Department of Aerospace and Ocean Engineering

Virginia Polytechnic Institute and State University

Blacksburg, VA 24061

Abstract—This paper presents identification algorithms for a low-dimensional planar flow model composed of a uniform flow component and a singular flow component. With the aim of improving navigation for small autonomous underwater vehicles operating in shallow water, we develop algorithms that can be performed in near real-time using small, sparse data sets. Although we compare several variations, the basic approach involves identifying the uniform flow component, the location of an assumed singularity, and the parameters which characterize the singular flow. In one variation, the flow model parameters are simply chosen to minimize a square error measure. In another variation, the minimization process is constrained to preserve the average divergence and circulation of the measured flow. The latter approach predictably results in a larger error, but produces a flow model which more realistically captures the flow in the larger region of the measurement points. Initial experimental results are presented.

I. INTRODUCTION

Models and model identification techniques for fluid flow have been developed for a wide range of applications, ranging from large-scale ocean flows [1] to particle-scale motion [2]. Driven by the stringent navigational requirements of autonomous underwater vehicles (AUVs) in shallow water applications (e.g. coastal, estuarine, and riverine), we seek to develop two-dimensional fluid flow models and associated identification algorithms. Our goal is to compute a fluid flow model using a small set of flow velocity estimates collected by a platoon of miniature AUVs. With such a model, the vehicles can compensate for the effect of fluid flow in mission planning and navigation in the region where the measurements were taken. By adopting a simple model, we trade model fidelity for near real-time identification using small, sparse data sets.

For oceanographic applications, image sequence processing [3] can quantify large-scale fluid motion. Deviations in successive satellite images are analyzed in order to assign a fluid velocity to each of a number of pixels. Depending on the image resolution and the chosen time interval, this technique provides a dense set of fluid velocity estimates that is used to develop and parametrize a two-dimensional flow model for surface currents. The fluid velocity estimates can be used to identify and isolate different rotational flow patterns [2].

Lagrangian coherent structures provide a technique of current interest in modeling time-varying fluid motion. Numerical algorithms, developed in [4] for example, perform well in identifying Lagrangian coherent structures, which resemble slowly time-varying stable and unstable manifolds in a phase portrait of a dynamical system. (In terms of fluid flow, stable manifolds attract fluid particles in forward time and unstable manifolds attract fluid particles in reverse time.) Methods for identifying Lagrangian coherent structures are intended to provide high fidelity, time-varying flow models of use to ocean scientists, rather than low-complexity, real-time flow estimates useful for short-term navigation.

In [5], an algorithm is proposed for identifying three-dimensional, time-invariant flow fields and is tested using data generated by computational fluid dynamics (CFD) simulations. The technique provides a reasonably high fidelity model of the fluid motion, but it requires a large number of flow field measurements.

Our goal for flow field identification is to improve the navigational performance of miniature AUVs that are typically not instrumented to measure current flow [6]. Since GPS-signals are not accessible underwater, the position of a submerged vehicle is estimated via dead-reckoning. Fluid flow affects the motion of the vehicle, leading to a navigational error. A pre-estimated flow field can be used to plan the vehicle's motion in a way that reduces this navigational error. When a vehicle resurfaces and obtains its current GPS position, the residual navigational error can be used to refine the flow field model. The number of flow field measurements required to implement this approach is quite small. For example, a platoon of four vehicles can identify a flow field by performing only two experimental dives each.

In Section II, a flow model is proposed that consists of a uniform flow component and a singular flow component. In general, the singular flow is a combination of a source/sink and a vortex. The algorithm to identify the unknown parameters in the model proceeds in four steps, as presented in Section III. Section III-A introduces estimation strategies for the uniform flow component. The location of the singularity is determined in Section III-B. A coordinate transformation, described in Section III-C, decomposes the flow field model and the measured flow field samples into dilatational (expanding or contracting) and rotational components. In Section III-D, least squares methods are used to minimize the error for the singular

flow identification. Two identification schemes are investigated and initial experimental are presented in Section IV.

II. PROBLEM STATEMENT AND FLOW FIELD MODEL

Similar to the approaches in [2] and [7], we assume the presence of a flow singularity which induces the regional fluid motion. We propose the following flow field model that assigns a flow velocity vector $\mathbf{V} = [V_x, V_y]^T \in \mathbb{R}^2$ to any point $\mathbf{r} = [x, y]^T \in \mathbb{R}^2$ in the horizontal plane

$$\mathbf{V}(\mathbf{r}) = \mathbf{U} + \mathbf{A}(\mathbf{r} - \mathbf{r}_s)w(\rho) \quad (1)$$

The constant vector $\mathbf{U} = [U_x, U_y]^T \in \mathbb{R}^2$ represents a uniform component of flow superimposed over the singular flow. The constant matrix

$$\mathbf{A} = \begin{bmatrix} a_{11} & a_{12} \\ a_{21} & a_{22} \end{bmatrix}$$

defines the flow pattern due to a flow singularity located at the fixed point $\mathbf{r}_s \in \mathbb{R}^2$. The function $w : \mathbb{R} \mapsto \mathbb{R}$ is introduced to weaken the singular flow component with increasing distance $\rho = \|\mathbf{r} - \mathbf{r}_s\|$. Choosing $w(\rho) = 1/\rho$, for example, will bound the flow field magnitude within the entire domain.

To simplify the discussion of singular flow, we define the alternative flow field model

$$\mathbf{V}_s(\mathbf{r}) = \mathbf{U} + \mathbf{A}(\mathbf{r} - \mathbf{r}_s) \quad (2)$$

(Equivalently, assume that $w(\rho) = 1$ in the definition (1).) The divergence of \mathbf{V}_s is given by the trace of the singularity matrix \mathbf{A} :

$$\text{div}(\mathbf{V}_s) = \frac{\partial}{\partial x} V_{s,x} + \frac{\partial}{\partial y} V_{s,y} = a_{11} + a_{22}$$

If the divergence is positive, then the singularity is a source. If it is negative, the singularity is a sink. The special case when $a_{11} = -a_{22}$ corresponds to a divergence free, purely rotational flow field.

The rotation of \mathbf{V}_s , or horizontal vorticity [8], is

$$\text{curl}(\mathbf{V}_s) = \frac{\partial}{\partial x} V_{s,y} - \frac{\partial}{\partial y} V_{s,x} = a_{21} - a_{12}$$

Thus, the skew elements of \mathbf{A} characterize the rotation of the flow. A positive horizontal vorticity $a_{21} > a_{12}$ describes counter-clockwise rotation and vice versa. For an irrotational motion induced by a pure sink or source, the singularity matrix satisfies $a_{12} = a_{21}$.

Divergence and vorticity play an important role in characterizing fluid flow. As intrinsic flow features, they provide a physical basis for identifying the elements of \mathbf{A} .

III. IDENTIFICATION

Identifying the flow field model (1), for a given choice of weakening function $w(\rho)$, requires one to determine eight unknown parameters: the components of \mathbf{U} , \mathbf{A} , and \mathbf{r}_s .

A data set containing N local flow velocity measurements at specific locations is assumed to be given. These measurements might be obtained, for example, using a platoon of small AUVs. Consider the following scenario. Each vehicle begins and ends its trajectory on the surface, where GPS signals are available, but performs the remainder of its trajectory below

the surface at some common, specified depth. Since GPS signals are not accessible to submerged AUVs, the submerged portion of the trajectory $r(t) = [x(t), y(t)]^T$ is estimated using a kinematic model

$$\begin{bmatrix} \dot{x} \\ \dot{y} \end{bmatrix} = \begin{bmatrix} \cos \psi \\ \sin \psi \end{bmatrix} \hat{u}_1 + \begin{bmatrix} V_x \\ V_y \end{bmatrix} \quad (3)$$

where ψ is the heading angle and \hat{u}_1 is the water relative longitudinal speed. We assume that the water relative motion is purely longitudinal, a reasonable assumption for steady state motion of a vehicle with good directional stability. Small AUVs typically do not carry sophisticated flow sensors, in any case; water relative longitudinal speed may instead be inferred from propeller rate.

The ambient flow field $\mathbf{V} = [V_x, V_y]^T$ influences the motion of the vehicle. In the kinematic model (3), the vehicle is simply assumed to drift with the current. Once again, the assumption is reasonable for a vehicle in steady motion; a trajectory involving extensive maneuvering may require a more sophisticated, dynamic model of the vehicle motion.

With no *a priori* knowledge of the ambient fluid motion, \mathbf{V} may be set to zero in equation (3) in order to obtain a best estimate of the vehicle's trajectory. Because of the ambient flow, this "dead reckoning" approach will generally result in a discrepancy between the predicted final position and the actual final position, as measured using GPS. We use this discrepancy to estimate the ambient flow along a given vehicle's trajectory. Given a collection of such estimates, we may then identify the parameters of the flow field model (1). Although other sources of dead reckoning errors will be present in practice, they are not addressed herein.

A. Uniform Flow

We assume that N flow velocity estimates \mathbf{V}_i are available, each corresponding to a measurement location \mathbf{P}_i , where $i \in \{1, \dots, N\}$. The uniform flow component \mathbf{U} may be treated in at least two different ways. One approach is to average over the sample set to obtain

$$\mathbf{U} = \frac{1}{N} \sum_{i=1}^N \mathbf{V}_i \quad (4)$$

Alternatively, one may simply assume that $\mathbf{U} = [0, 0]^T$ and seek a flow singularity which best reproduces the measured sample vectors. Both methods for defining \mathbf{U} are discussed with respect to experimental results in Section IV-A.

B. Localization of a Flow Singularity

Having defined \mathbf{U} , by either of the methods described in Section III-A, one may proceed to identify the remaining singular flow model

$$\begin{aligned} \tilde{\mathbf{V}}(\mathbf{r}) &:= \mathbf{V}(\mathbf{r}) - \mathbf{U} \\ &= \mathbf{A}(\mathbf{r} - \mathbf{r}_s)w(\rho) \end{aligned} \quad (5)$$

The first step is to determine the location \mathbf{r}_s of the assumed flow singularity which induces the flow $\tilde{\mathbf{V}}(\mathbf{r})$. To determine this location, we use the residual flow velocity measurements

$$\tilde{\mathbf{V}}_i = \mathbf{V}_i - \mathbf{U} \quad (6)$$

Definition. The geometric center of measurements is

$$\mathbf{P}_{\text{cm}} = \frac{1}{N} \sum_{i=1}^N \mathbf{P}_i. \quad (7)$$

Proposition 3.1: Consider a set of N velocity measurements \mathbf{V}_i and suppose that the uniform flow component \mathbf{U} has been computed as in (4) and removed as in (6) to produce a set of N residual velocity measurements $\tilde{\mathbf{V}}_i$. Further, suppose that these residual velocity measurements satisfy (5) identically for some nonsingular matrix \mathbf{A} , with $w(\rho) = 1$. Then $\mathbf{r}_s = \mathbf{P}_{\text{cm}}$.

Proof: By assumption, each residual velocity estimate $\tilde{\mathbf{V}}_i$ satisfies

$$\tilde{\mathbf{V}}_i = \mathbf{A}(\mathbf{P}_i - \mathbf{r}_s).$$

Summing over i and dividing by N gives

$$\begin{aligned} \frac{1}{N} \sum_{i=1}^N \tilde{\mathbf{V}}_i &= \frac{1}{N} \sum_{i=1}^N \mathbf{A}(\mathbf{P}_i - \mathbf{r}_s) \\ &= \mathbf{A} \frac{1}{N} \sum_{i=1}^N (\mathbf{P}_i - \mathbf{r}_s) \end{aligned}$$

But (4) and (6) imply that

$$\frac{1}{N} \sum_{i=1}^N \tilde{\mathbf{V}}_i = \mathbf{0}$$

Because \mathbf{A} is nonsingular, by assumption, we find

$$\begin{aligned} \mathbf{0} &= \frac{1}{N} \sum_{i=1}^N (\mathbf{P}_i - \mathbf{r}_s) \\ &= \frac{1}{N} \left(\sum_{i=1}^N \mathbf{P}_i \right) - \mathbf{r}_s. \end{aligned}$$

It follows that

$$\mathbf{r}_s = \frac{1}{N} \sum_{i=1}^N \mathbf{P}_i = \mathbf{P}_{\text{cm}} \quad \square$$

Thus, assuming that the flow model (2) accurately characterizes the flow measurements, the singularity location is the center of measurements. A similar statement holds when one includes a weakening function $w(\rho)$. In the general case, one finds that

$$\mathbf{r}_s = \mathbf{P}_{\text{cm}} + \frac{\sum_{i=1}^N (\mathbf{P}_i - \mathbf{r}_s) w(\|\mathbf{P}_i - \mathbf{r}_s\|)}{\sum_{i=1}^N w(\|\mathbf{P}_i - \mathbf{r}_s\|)}$$

Because of the weighting function $w(\cdot)$, finding the singularity location \mathbf{r}_s by this approach will generally require one to solve a nonlinear algebraic equation, which must typically be done using numerical methods. For the specific choice $w(\rho) = \frac{1}{\rho}$, one can show that the singularity must be located within the convex hull of the measurement locations, provided it is well defined. This observation bounds the region to be searched using a numerical root finding technique.

The approach described above for locating the singularity is somewhat dissatisfying, though, in that it appears to take no account of the flow measurements themselves. In reality, the measurements are accounted for when one computes the uniform flow component. Still, at this early point in the flow identification process, assuming that the residual flow measurements satisfy (5) identically seems overly restrictive.

Figure 1 illustrates a different approach for locating the assumed flow singularity. For any candidate singularity location $\mathbf{r} = [x, y]^T$, the angles $\theta_i(\mathbf{r})$ between the vectors $\mathbf{r} - \mathbf{P}_i$

and the residual flow measurements $\tilde{\mathbf{V}}_i$ can be computed. These angles, evaluated in four quadrants, correlate to the surrounding flow pattern and are defined by the geometric relations

$$\begin{aligned} \sin \theta_i(\mathbf{r}) &= \frac{(\mathbf{r} - \mathbf{P}_i) \times \tilde{\mathbf{V}}_i}{\|\tilde{\mathbf{V}}_i\| \|\mathbf{r} - \mathbf{P}_i\|} \cdot \mathbf{e}_z = \frac{(x - P_{i,x})\tilde{V}_{y,i} - (y - P_{i,y})\tilde{V}_{x,i}}{\|\tilde{\mathbf{V}}_i\| \|\mathbf{r} - \mathbf{P}_i\|} \\ \cos \theta_i(\mathbf{r}) &= \frac{(\mathbf{r} - \mathbf{P}_i) \cdot \tilde{\mathbf{V}}_i}{\|\tilde{\mathbf{V}}_i\| \|\mathbf{r} - \mathbf{P}_i\|} = \frac{(x - P_{i,x})\tilde{V}_{x,i} + (y - P_{i,y})\tilde{V}_{y,i}}{\|\tilde{\mathbf{V}}_i\| \|\mathbf{r} - \mathbf{P}_i\|} \end{aligned} \quad (8)$$

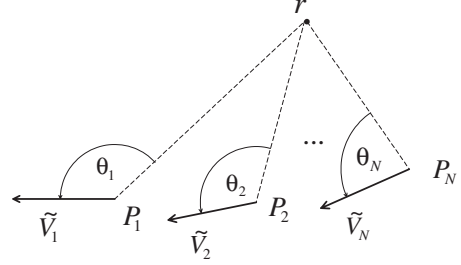


Fig. 1. Evaluation of the singular flow pattern around \mathbf{r} .

In [2], every location \mathbf{r} that satisfies $\theta_i = 90^\circ$ for all sample vectors is considered as a singularity location of a clockwise vortex. A similar statement holds for a counter-clockwise vortex with $\theta_i = -90^\circ$. We expand the approach to include dilatation, as well as rotation. For a source, for example, $\theta_i = 180^\circ$ while for a sink $\theta_i = 0^\circ$. Associated with these four classifications are four cost functions Γ_j , $j = 1, \dots, 4$, defined to evaluate how well \mathbf{r} represents a singularity of a corresponding type:

$$\begin{aligned} \text{sink} & \Gamma_1(\mathbf{r}) = \sum_{i=1}^N (\cos \theta_i - 1)^2 \\ \text{source} & \Gamma_2(\mathbf{r}) = \sum_{i=1}^N (\cos \theta_i + 1)^2 \\ \text{clockwise vortex} & \Gamma_3(\mathbf{r}) = \sum_{i=1}^N (\sin \theta_i - 1)^2 \\ \text{counter-clockwise vortex} & \Gamma_4(\mathbf{r}) = \sum_{i=1}^N (\sin \theta_i + 1)^2 \end{aligned} \quad (9)$$

In the definitions (9), $\Gamma_j(\mathbf{r}) : \mathbb{R}^2 \setminus \mathbb{M} \mapsto \mathbb{R}$, where $\mathbb{M} = \{\mathbf{r} \mid \|\mathbf{r} - \mathbf{P}_i\| < \delta, i = 1 \dots N\}$ contains δ -neighborhoods of each measurement location \mathbf{P}_i (for which the angle θ_i is not defined). The radius $\delta > 0$ can be chosen arbitrarily small, but should be non-zero.

The best choices for singularity locations are the minima of $\Gamma_j(\mathbf{r})$. By definition, the cost functions are continuously differentiable in $\mathbb{R}^2 \setminus \mathbb{M}$. Thus, a gradient descent approach can be applied to each $\Gamma_j(\mathbf{r})$ in order to determine the respective local minima

$$\dot{\mathbf{r}}_j(t) = -\gamma_j(t) \text{grad} \Gamma_j(\mathbf{r}_j) \quad \text{with} \quad j = 1..4 \quad (10)$$

The four trajectories $\mathbf{r}_j(t)$ evolve separately from a joint initial position $\mathbf{r}_{0,j} = \mathbf{P}_{\text{cm}}$, see (7). The adaptive step sizes $\gamma_j(t)$ with $\gamma_{max} \geq \gamma_j(t) \geq \gamma_{min} > 0$ provide a trade-off between high accuracy of the algorithm versus computational time. They can be adjusted as $\mathbf{r}_j(t)$ evolves.

At present, convergence of (10) is not guaranteed for all possible sets of sample vectors and remains as an open

research question. For a restricted range of initial conditions, however, a gradient method (10) can be proven to converge to the desired local minimum.

Proposition 3.2: Assume that there exists a unique minimum at $\mathbf{r}_{s,j}$ in a neighborhood

$$\mathbb{B}_j = \{\mathbf{r} \in \mathbb{R}^2 \setminus \mathbb{M} \mid \|\mathbf{r} - \mathbf{r}_{s,j}\| \leq \epsilon\}$$

where ϵ is sufficiently small so that \mathbb{B}_j does not contain elements of \mathbb{M} . Also assume that

$$\text{grad} \Gamma_j(\mathbf{r}_j) \neq 0 \quad \forall \mathbf{r}_j \in \mathbb{B}_j, \mathbf{r}_j \neq \mathbf{r}_{s,j}.$$

Then, for any initial condition $\mathbf{r}_{0,j} \in \mathbb{B}_j$, the gradient method (10) will converge to $\mathbf{r}_{s,j}$.

For experimental data, the gradient method (10) generally converges for more than one cost function. Thus, there is more than one choice of singularity location and type. The impact of such a choice is discussed in Section IV-A.

Rather than restrict the form of \mathbf{A} to represent a pure singularity, we take the identified location $\mathbf{r}_{s,j}$ to be the center of a more general flow singularity. For example, in considering the candidate singularity location of a vortex (Γ_3 or Γ_4), we do not assume that the flow is purely rotational.

C. Polar Representation of the Flow Field Model

To identify the singularity matrix \mathbf{A} , a transformation of the flow field model (5) to polar coordinates is considered. Under the assumption that the singularity location is known, from Section III-B, a polar coordinate system with the origin at $\mathbf{r}_s = [x_s, y_s]^T$ provides a more concise mathematical representation of the singular flow, one which naturally decomposes the flow field model and measurement vectors into rotational and dilatational components. Define the angle φ by the expression

$$\tan \varphi = \frac{y - y_s}{x - x_s}$$

where it $\varphi \in [0, 2\pi)$. Recalling the definition $\rho = \|\mathbf{r} - \mathbf{r}_s\|$, one finds the singular flow (5) in polar coordinate representation

$$\tilde{\mathbf{V}}(\rho, \varphi) = \tilde{V}_\rho(\rho, \varphi) \mathbf{e}_\rho + \tilde{V}_\varphi(\rho, \varphi) \mathbf{e}_\varphi \quad (11)$$

where \mathbf{e}_ρ and \mathbf{e}_φ are the unit vectors corresponding to the radial and angular directions, respectively. The vector components are

$$\begin{aligned} \tilde{V}_\rho(\rho, \varphi) &= w(\rho) \rho [a_{11}c^2\varphi + a_{22}s^2\varphi + (a_{12} + a_{21})s\varphi c\varphi] \\ \tilde{V}_\varphi(\rho, \varphi) &= w(\rho) \rho [a_{21}c^2\varphi - a_{12}s^2\varphi + (a_{22} - a_{11})s\varphi c\varphi] \end{aligned} \quad (12)$$

where $c\varphi := \cos \varphi$ and $s\varphi := \sin \varphi$.

Note in (12) that choosing $w(\rho) = \frac{1}{\rho}$ cancels the dependency of $\tilde{\mathbf{V}}(\rho, \varphi)$ on ρ . Thus, the singular flow field model (11) is distance invariant. We omit the argument ρ from the components of the flow field model:

$$\tilde{V}_\rho(\varphi) := \tilde{V}_\rho(\rho, \varphi) \quad \text{and} \quad \tilde{V}_\varphi(\varphi) := \tilde{V}_\varphi(\rho, \varphi)$$

While fixing the form of $w(\rho)$ limits the versatility of the flow field model somewhat, the choice $w(\rho) = \frac{1}{\rho}$ bounds the magnitude of the flow vectors in \mathbb{R}^2 . The result is a more physically intuitive flow model that may even be useful outside the immediate vicinity of the flow measurements. Moreover,

sufficient freedom remains in the model to capture intrinsic flow characteristics, such as divergence and circulation, in the region where measurements are made.

The expressions in (12) may be rewritten as

$$\begin{bmatrix} \tilde{V}_\rho(\varphi) \\ \tilde{V}_\varphi(\varphi) \end{bmatrix} = \begin{bmatrix} \mathbf{b}_\rho^T(\varphi) \\ \mathbf{b}_\varphi^T(\varphi) \end{bmatrix} \mathbf{p} \quad (13)$$

where

$$\begin{aligned} \mathbf{b}_\rho^T(\varphi) &= \begin{bmatrix} \cos 2\varphi & \sin 2\varphi & 1 & 0 \end{bmatrix}, \\ \mathbf{b}_\varphi^T(\varphi) &= \begin{bmatrix} -\sin 2\varphi & \cos 2\varphi & 0 & 1 \end{bmatrix} \end{aligned}$$

and

$$\mathbf{p} = \begin{bmatrix} p_1 \\ p_2 \\ p_3 \\ p_4 \end{bmatrix} = \frac{1}{2} \begin{bmatrix} 1 & 0 & 0 & -1 \\ 0 & 1 & 1 & 0 \\ 1 & 0 & 0 & 1 \\ 0 & -1 & 1 & 0 \end{bmatrix} \begin{bmatrix} a_{11} \\ a_{12} \\ a_{21} \\ a_{22} \end{bmatrix} \quad (14)$$

Note that identifying the new parameter vector \mathbf{p} is equivalent to identifying \mathbf{A} .

D. Singular Flow Identification

A technique that determines the parameters \mathbf{p} and thus the singularity matrix \mathbf{A} is presented in this section. The goal is to approximate the measured flow field vectors using the proposed model by minimizing the root-mean-squared error

$$\eta(\mathbf{V}_i, \mathbf{V}) = \sqrt{\frac{1}{N} \sum_{i=1}^N \|\mathbf{V}_i - \mathbf{V}(\mathbf{P}_i)\|^2} \quad (15)$$

(Note: \mathbf{V}_i is the flow measured at \mathbf{P}_i whereas $\mathbf{V}(\mathbf{P}_i)$ is the flow model (1) evaluated at \mathbf{P}_i .) After the uniform flow \mathbf{U} and the singularity location \mathbf{r}_s are determined, minimizing η^2 becomes a linear least squares problem. Thus, one can directly obtain \mathbf{A} by minimizing

$$\begin{aligned} \eta^2(\mathbf{V}_i, \mathbf{V}) &= \frac{1}{N} \sum_{i=1}^N \|\mathbf{V}_i - \left(\mathbf{U} + \frac{1}{\rho_i} \mathbf{A}(\mathbf{r}_s - \mathbf{P}_i)\right)\|^2 \\ &= \frac{1}{N} \sum_{i=1}^N \|\tilde{\mathbf{V}}_i - \frac{1}{\rho_i} \mathbf{A}(\mathbf{r}_s - \mathbf{P}_i)\|^2. \end{aligned} \quad (16)$$

More generally, one may instead minimize

$$\begin{aligned} J &= \sum_{i=1}^N \left[q_{i,\rho} \left(\tilde{V}_\rho(\varphi_i) - \tilde{V}_{i,\rho} \right)^2 \dots \right. \\ &\quad \left. + q_{i,\varphi} \left(\tilde{V}_\varphi(\varphi_i) - \tilde{V}_{i,\varphi} \right)^2 \right] \\ &= \sum_{i=1}^N \left[q_{i,\rho} \left(\mathbf{b}_\rho^T(\varphi_i) \mathbf{p} - \tilde{V}_{i,\rho} \right)^2 \dots \right. \\ &\quad \left. + q_{i,\varphi} \left(\mathbf{b}_\varphi^T(\varphi_i) \mathbf{p} - \tilde{V}_{i,\varphi} \right)^2 \right] \end{aligned} \quad (17)$$

where the weight coefficients $q_{i,\rho}$ and $q_{i,\varphi}$ may be adjusted to emphasize dilatational or rotational flow, whichever is suggested by the data.

Suppose we stack the dilatational and rotational components of the measurement vectors and the parameter coefficients \mathbf{b}_ρ and \mathbf{b}_φ as follows

$$\begin{aligned} \mathbf{W}^T &= \left[\tilde{V}_{i,\rho}(\varphi_i), \dots, \tilde{V}_{i,\rho}(\varphi_N), \tilde{V}_{i,\varphi}(\varphi_i), \dots, \tilde{V}_{i,\varphi}(\varphi_N) \right] \\ \mathbf{B}^T &= \left[\mathbf{b}_\rho^T(\varphi_i), \dots, \mathbf{b}_\rho^T(\varphi_N), \mathbf{b}_\varphi^T(\varphi_i), \dots, \mathbf{b}_\varphi^T(\varphi_N) \right] \end{aligned}$$

and define the diagonal weighting matrix

$$\mathbf{Q} = \text{diag}(q_{1,\rho} \dots q_{N,\rho}, q_{1,\varphi} \dots q_{N,\varphi})$$

The solution \mathbf{p} of the equation

$$\mathbf{Q}(\mathbf{B}\mathbf{p} - \mathbf{W}) = \mathbf{0} \quad (18)$$

which minimizes J is

$$\mathbf{p} = \mathbf{B}_Q^\dagger \mathbf{Q} \mathbf{W} \quad (19)$$

where \mathbf{B}_Q^\dagger is the weighted Moore-Penrose matrix pseudo inverse

$$\mathbf{B}_Q^\dagger = (\mathbf{B}^T \mathbf{Q} \mathbf{B})^{-1} \mathbf{B}^T$$

The singularity matrix \mathbf{A} is obtained from (14).

Experimental results discussed in Section IV-A (with \mathbf{Q} chosen as the identity matrix) show that minimizing η yields a suitable flow field representation in the immediate region of the measurements. The larger regional flow may not be as accurately characterized, however. Depending on the application, capturing the regional flow characteristics may have a higher priority than minimizing the identification error η . In AUV applications, for example, it may occasionally be necessary to navigate beyond the region of existing flow measurements. A flow field model which accurately reproduces intrinsic features of the flow, such as dilatation and rotation, may provide a better representation of the actual flow over a larger region. In the following, we discuss a trade-off between these two objectives: high accuracy and a feasible representation of the larger-scale flow pattern.

Natural flow phenomena, such as upwellings and swirling flow described in [8], justify using average divergence and horizontal vorticity to partially describe a planar flow. In the proposed method, estimates of these quantities are obtained directly from the flow field samples. The average divergence and horizontal vorticity are then reproduced by the flow field model discussed in Section II.

In polar coordinates, the divergence of the flow field model (11) is [10]

$$\begin{aligned} \text{div}(\tilde{\mathbf{V}}) &= \frac{1}{\rho} \frac{\partial}{\partial \rho}(\rho \tilde{V}_\rho) + \frac{1}{\rho} \frac{\partial}{\partial \varphi} \tilde{V}_\varphi \\ &= \frac{1}{\rho} \begin{bmatrix} -\cos 2\varphi & -\sin 2\varphi & 1 & 0 \end{bmatrix} \mathbf{p} \end{aligned} \quad (20)$$

For the proposed flow field model, an average divergence $\overline{\text{div}(\mathbf{V})}$ per unit area is considered. Define a horizontal disc $\mathbb{A} = \{(\rho, \varphi) \mid \rho \leq \rho_\mathbb{A}, \varphi \in [0, 2\pi)\}$ with the radius $\rho_\mathbb{A}$ centered at the singularity. The area is $A_\mathbb{A} = \pi \rho_\mathbb{A}^2$ and a differential area element is $d\mathbb{A} = \rho d\rho d\varphi$. The radius $\rho_\mathbb{A}$ is chosen sufficiently large that \mathbb{A} contains all flow velocity measurements. The average divergence per unit area is

$$\begin{aligned} \overline{\text{div}(\mathbf{V})} &= \frac{1}{A_\mathbb{A}} \int_{\mathbb{A}} \text{div}(\tilde{\mathbf{V}}) d\mathbb{A} \\ &= \frac{1}{\pi \rho_\mathbb{A}^2} \int_0^{\rho_\mathbb{A}} \int_0^{2\pi} \text{div}(\tilde{\mathbf{V}}) \rho d\varphi d\rho \\ &= \frac{2}{\rho_\mathbb{A}} p_3 \end{aligned} \quad (21)$$

Thus, $\overline{\text{div}(\mathbf{V})}$ is directly proportional to the parameter $p_3 = \frac{1}{2}(a_{11} + a_{22})$.

Evaluating partial derivatives (20) in order to compute $\text{div}(\tilde{\mathbf{V}})$ and to estimate p_3 in (21) does not seem feasible for a small, sparse set of measurement vectors. This issue is circumvented by using Gauss' integral theorem of divergence:

$$\int_{\mathbb{A}} \text{div}(\tilde{\mathbf{V}}) d\mathbb{A} = \oint_{\mathbf{S}} \tilde{\mathbf{V}} \cdot d\mathbf{S}_\perp \quad (22)$$

where $d\mathbf{S}_\perp$ is the unit normal to the closed curve $\mathbf{S} = \{(\rho, \varphi) \mid \rho = \rho_\mathbb{A}, \varphi \in [0, 2\pi)\}$, which encloses \mathbb{A} , at a given angle φ . Applying Gauss' integral theorem to (21) yields

$$\begin{aligned} \overline{\text{div}(\mathbf{V})} &= \frac{1}{A_\mathbb{A}} \oint_{\mathbf{S}} \tilde{\mathbf{V}} \cdot d\mathbf{S}_\perp \\ &= \frac{1}{\pi \rho_\mathbb{A}^2} \int_0^{2\pi} [\tilde{V}_\rho \mathbf{e}_\rho + \tilde{V}_\varphi \mathbf{e}_\varphi] \cdot (\rho_\mathbb{A} d\varphi \mathbf{e}_\rho) \\ &= \frac{2}{\rho_\mathbb{A}} \frac{1}{2\pi} \int_0^{2\pi} \tilde{V}_\rho d\varphi \end{aligned} \quad (23)$$

Assuming that the residual measured flow velocities are induced by the proposed singular flow model (5), equation (23) may be used to approximate the average divergence $\overline{\text{div}(\mathbf{V})}$ using the dilatational parts of $\tilde{\mathbf{V}}_i$. Comparing coefficients in (21) and (23) gives

$$p_3 = \frac{1}{2\pi} \int_0^{2\pi} \tilde{V}_\rho d\varphi$$

Because sample vectors will not generally be available along the entire circle \mathbf{S} , the following approximation is used:

$$p_3 = \bar{V}_\rho := \frac{1}{N} \sum_{i=1}^N \tilde{V}_{i,\rho} \quad (24)$$

where $\tilde{V}_{i,\rho}$ is the radial component of the residual data vector $\tilde{\mathbf{V}}_i$. This approximation is well-justified if the divergence remains nearly constant within the sample set.

Next, consider the rotation of (11)

$$\begin{aligned} \text{curl}(\tilde{\mathbf{V}}) &= \frac{1}{\rho} \frac{\partial}{\partial \rho}(\rho \tilde{V}_\varphi) - \frac{1}{\rho} \frac{\partial}{\partial \varphi} \tilde{V}_\rho \\ &= \frac{1}{\rho} \begin{bmatrix} \sin 2\varphi & -\cos 2\varphi & 0 & 1 \end{bmatrix} \mathbf{p} \end{aligned}$$

The average rotation per unit area is

$$\begin{aligned} \overline{\text{curl}(\mathbf{V})} &= \frac{1}{A_\mathbb{A}} \int_{\mathbb{A}} \text{curl}(\tilde{\mathbf{V}}) \cdot \mathbf{e}_z d\mathbb{A} \\ &= \frac{1}{\pi \rho_\mathbb{A}^2} \int_0^{\rho_\mathbb{A}} \int_0^{2\pi} \text{curl}(\tilde{\mathbf{V}}) \cdot \mathbf{e}_z \rho d\rho d\varphi \\ &= \frac{2}{\rho_\mathbb{A}} p_4 \end{aligned} \quad (25)$$

Adopting Stoke's integral theorem of rotation

$$\int_{\mathbb{A}} \text{curl}(\tilde{\mathbf{V}}) \cdot \mathbf{e}_z d\mathbb{A} = \oint_{\mathbf{S}} \tilde{\mathbf{V}} \cdot d\mathbf{S}$$

yields

$$\begin{aligned} \overline{\text{curl}(\mathbf{V})} &= \frac{1}{A_\mathbb{A}} \oint_{\mathbf{S}} \tilde{\mathbf{V}} \cdot d\mathbf{S} \\ &= \frac{1}{\pi \rho_\mathbb{A}^2} \int_0^{2\pi} [\tilde{V}_\rho \mathbf{e}_\rho + \tilde{V}_\varphi \mathbf{e}_\varphi] \cdot (\rho_\mathbb{A} d\varphi \mathbf{e}_\varphi) \\ &= \frac{2}{\rho_\mathbb{A}} \frac{1}{2\pi} \int_0^{2\pi} \tilde{V}_\varphi d\varphi \end{aligned} \quad (26)$$

From (25) and (26), we conclude that

$$p_4 = \frac{1}{2\pi} \int_0^{2\pi} \tilde{V}_\varphi d\varphi$$

Thus, approximating p_4 as

$$p_4 = \bar{V}_\varphi := \frac{1}{N} \sum_{i=1}^N \tilde{V}_{i,\varphi} \quad (27)$$

captures the regional rotation of the flow.

The approximations $p_3 = \bar{V}_\rho$ and $p_4 = \bar{V}_\varphi$ reduce the number of parameters that remain to be identified. The cost function (17), with the pre-determined parameters \bar{V}_ρ and \bar{V}_φ , becomes

$$\tilde{J} = \sum_{i=1}^N \left[\begin{array}{l} q_{i,\rho} \left(\mathbf{b}_\rho^T(\varphi_i) [p_1 \ p_2 \ 0 \ 0]^T + \bar{V}_\rho - \tilde{V}_{i,\rho} \right)^2 \dots \\ + q_{i,\varphi} \left(\mathbf{b}_\varphi^T(\varphi_i) [p_1 \ p_2 \ 0 \ 0]^T + \bar{V}_\varphi - \tilde{V}_{i,\varphi} \right)^2 \end{array} \right] \quad (28)$$

which can be solved similarly to (18). Of course, removing the free parameters p_3 and p_4 will generally result in a larger minimum value of \tilde{J} than of J . Minimizing \tilde{J} , however, is more physically inspired and produces flow models that appear valid beyond the immediate region of flow measurements.

The two strategies to identify the singular flow, by either using a least squares approach for all four parameters p_1, \dots, p_4 or matching regional fluid characteristics by selecting p_3 and p_4 accordingly, are compared in Section IV using experimental data.

IV. EXPERIMENTAL RESULTS

The flow field identification algorithm is applied to a set of data that was collected during field experiments in the Lafayette river near Norfolk, Virginia [11]. In the field experiment, a single vehicle was commanded to operate on the surface, so that GPS position updates could be obtained along the entire trajectory. While AUVs are normally submerged, the experiment was conducted in this manner to provide ground truth for the AUV trajectory. Position updates were collected every 30 seconds. Between each two successive position measurements, the kinematic model (3) was utilized to estimate the trajectory. The error between the true and predicted final position was used to estimate the fluid flow velocity \mathbf{V}_i along that segment. (The flow velocity was assumed to be uniform along each segment.) Figure 2 shows the GPS data and the extracted flow velocity measurements. GPS-tracked surface drifters were deployed simultaneously [12]. Assuming that the drifters followed the true flow, their GPS tracks provide at least a qualitative measure of a given flow model's accuracy. The performance of the flow field model (1) is examined for several proposed variations of the algorithm described in Section III.

In Section IV-A, all four parameters of the flow singularity matrix \mathbf{A} were identified by minimizing the cost function (17). In one case, we assume that there is a nonzero component of uniform flow $\mathbf{U} \neq \mathbf{0}$, while in another we assume that $\mathbf{U} = \mathbf{0}$. In the former case, the singularity localization algorithm (10) is applied to the cost functions Γ_j^* that utilize the residual flow velocity measurements $\tilde{\mathbf{V}}_i$, see (6). In this case, as

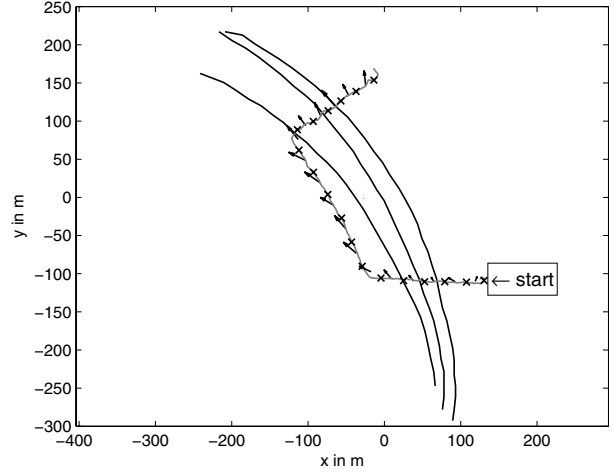


Fig. 2. GPS way points 'x' along the vehicle's trajectory are utilized to extract the local flow measurements ' $\tilde{\mathbf{V}}_i$ '. The drifter tracks ' $\tilde{\mathbf{V}}_i$ ' are used as comparison to evaluate the performance of the identification algorithm.

discussed in Section III-B, a flow singularity is detected at $\mathbf{r}_{s,2}$ inside the convex hull of the measurement locations. In the latter case $\mathbf{U} = \mathbf{0}$, we find $\tilde{\mathbf{V}}_i = \mathbf{V}_i$. Thus, the flow velocity measurements \mathbf{V}_i and the respective cost functions Γ_j^* are considered to find singularity candidates. (The superscript asterisk distinguishes the case $\mathbf{U} = \mathbf{0}$ from $\mathbf{U} \neq \mathbf{0}$, for which the residual data set is different.) The singularity localization algorithm suggests two locations $\mathbf{r}_{s,4}^*$ and $\mathbf{r}_{s,2}^*$.

An alternative approach for the singular flow identification is presented in Section IV-B. For this case, we select $\mathbf{U} = \mathbf{0}$ and the singularity candidate at $\mathbf{r}_{s,4}^*$. The parameter vector \mathbf{p} of the singular flow component is identified using average divergence (24) and horizontal vorticity measures (27), while p_1 and p_2 minimize (28). The corresponding approach with $\mathbf{U} \neq \mathbf{0}$ is not investigated, since subtracting the uniform flow as in (6) yields residual flow velocity measurements $\tilde{\mathbf{V}}_i$ with a different inherent flow pattern than \mathbf{V}_i .

Table I summarizes the various modeling results.

TABLE I
IDENTIFICATION TECHNIQUES AND THE RESULTING FLOW FIELD MODELS.

flow identification	assumption	singular flow pattern	η in ms^{-1}
Sec. IV-A, Fig. 3	$\mathbf{U} \neq \mathbf{0}$	$\Gamma_2(\mathbf{r}_{s,2}) = 0.2027$	0.0882
Sec. IV-A, Fig. 4	$\mathbf{U} = \mathbf{0}$	$\Gamma_4^*(\mathbf{r}_{s,4}^*) = 0.0130$	0.1133
Sec. IV-A, Fig. 5	$\mathbf{U} = \mathbf{0}$	$\Gamma_2^*(\mathbf{r}_{s,2}^*) = 0.0027$	0.1173
Sec. IV-B, Fig. 6	$\mathbf{U} = \mathbf{0}$	$\Gamma_4^*(\mathbf{r}_{s,4}^*) = 0.0130$	0.1424

A. Least Squares Minimization

Case 1: $\mathbf{U} \neq \mathbf{0}$. As discussed in Section III-A, the uniform flow \mathbf{U} can be identified as the average over all flow velocity estimates (4). A singularity is detected at $\mathbf{r}_{s,2}$ and the singularity matrix \mathbf{A} corresponding to this location is identified using the least squares approach applied to the cost function (17). Figure 3 shows the identified singular flow component (5) in the left plot and the full flow field model (1)

in the right plot. Of the various approaches suggested, this approach yields the smallest RMS error η as defined in (15).

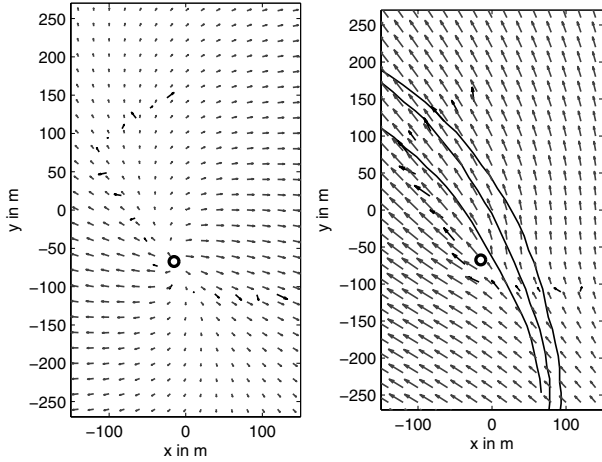


Fig. 3. Left plot: The singular flow $\tilde{\mathbf{V}}(\mathbf{r})$ is identified using the residual sample vectors $\tilde{\mathbf{V}}_i = \mathbf{V}_i - \mathbf{U}$. A source (represented by a 'o') is detected at $\mathbf{r}_{s,2}^*$. Right plot: The combined uniform and singular flow components.

Case 2: $\mathbf{U} = \mathbf{0}$. The same data set suggests alternate flow field models if one assumes that the flow is purely singular. Using this approach, two singularities are detected, a counter-clockwise vortex at $\mathbf{r}_{s,4}^*$ in Figure 4 and a source at $\mathbf{r}_{s,2}^*$ in Figure 5. In both cases, the singular flow is identified using the least squares approach applied to the cost function (17). Note, first of all, that the singularity $\mathbf{r}_{s,4}^*$ is located far outside the region in which the measurements are taken. When $\mathbf{U} = \mathbf{0}$, there is no guaranteed bounds on the candidate singularity locations. Also note, in Figure 4, that the flow characteristics change dramatically outside the immediate neighborhood of the measurements, with the flow reversing direction near the start of the drifter tracks. Both flow field models do not provide an intuitively reasonable estimate of the regional flow. The identification errors η in Table I are slightly larger for this case; this is to be expected, since setting $\mathbf{U} = \mathbf{0}$ eliminates two free parameters.

Comparing Figure 4 and Figure 5, one can see that the selection of the singularity location has a significant impact on the modeled flow pattern, although a noticeable difference in the identification error in Table I does not occur. A decision can be made by either imposing identification priorities, such as identifying a rotational flow pattern, or by selecting the singularity location associated with the lowest final cost Γ_j^* or with the lowest overall cost η .

B. Constrained Least Squares Minimization

In this section, the flow model is constrained to recover the average divergence and horizontal vorticity given by the flow velocity measurements, as proposed in Section III-D. Using this identification strategy, only the two remaining parameters p_1 and p_2 are determined by minimizing the modified cost function (28). The resulting flow field model is shown in Figure 6. Illustrated in Table I, this approach results in a

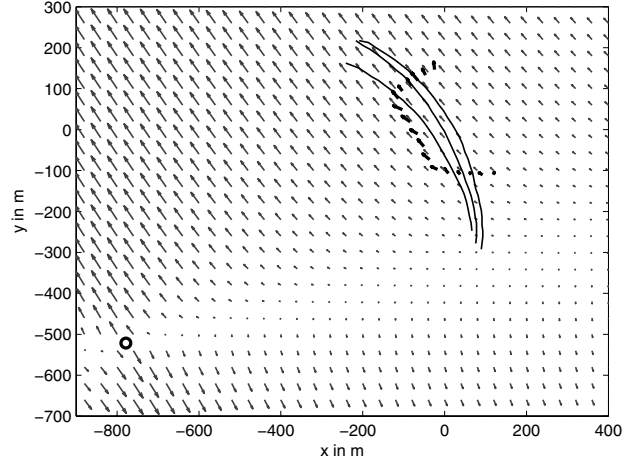


Fig. 4. The flow field is identified assuming a zero uniform flow. A counter-clockwise vortex (represented by a 'o') is detected at $\mathbf{r}_{s,4}^*$ and is chosen for the singular flow identification.

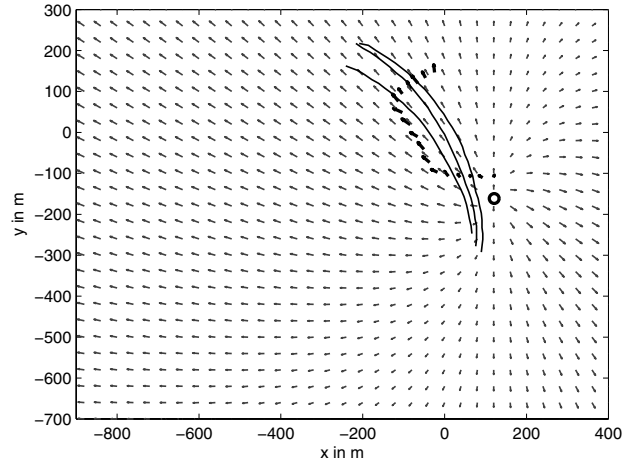


Fig. 5. The flow field is identified assuming a zero uniform flow. A source (represented by a 'o') is detected at $\mathbf{r}_{s,2}^*$ and is chosen for the singular flow identification.

slightly larger identification error compared to the approach illustrated in Figure 4 that presumes the same singularity location.

C. Summary of Experimental Results

Of the four approaches shown, there are potentially many factors that contribute to a selection of one solution over another. Based on the limited experimental work reported herein, we offer the following guideline: If regional flow characteristics of the flow are desired and should be preserved, then choose $\mathbf{U} = \mathbf{0}$ and the constrained 2-parameter estimation, which utilizes average vorticity and divergence. Otherwise, the flow field model that achieves the lowest identification error η should be selected. A non-zero uniform flow $\mathbf{U} \neq \mathbf{0}$ should be chosen, if it is essential that the modeled singularity appears in the smallest convex set that includes the data

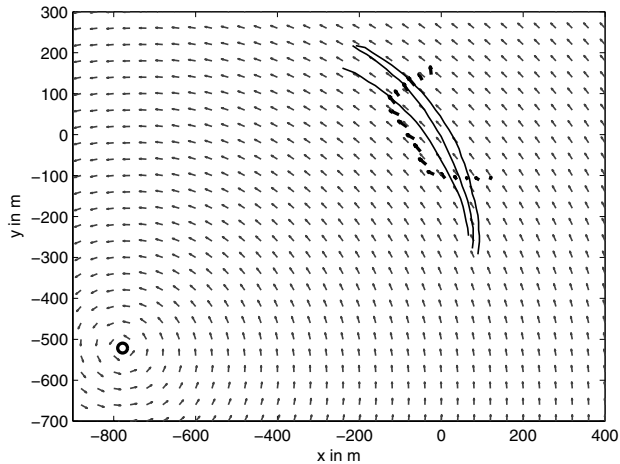


Fig. 6. The flow field is identified assuming a zero uniform flow. The counter-clockwise vortex at $\mathbf{r}_{s,4}^*$ is considered. The average divergence and vorticity are estimated from data and the resulting model is constrained to preserve these characteristics.

vectors. For navigational purposes, one might choose the lowest identification error if the AUV exclusively operates in the area where flow velocity measurements are available.

D. Application in AUV Navigation

Figure 7 illustrates the advantage of assessing the ambient fluid motion for AUV navigation. Based on the vehicle's estimated water relative velocity and the compass heading angle, the AUV's trajectory is recalculated using the kinematic model (3) with and without the modeled environmental flow field presented in Figure 6. The error of the predicted destination decreases from 34.1 percent of distance traveled (%DT) to 5.6 %DT. This improvement in navigational performance can improve position estimates associated with science measurements and can improve operational efficiency by allowing longer duration dives.

V. CONCLUSION AND FUTURE WORK

In this paper, we develop a technique to identify a proposed flow field model using a small, sparse set of flow velocity measurements collected by a platoon of AUVs. Standard optimization tools are adopted to ensure a minimal identification error. A gradient method detects candidate locations for flow singularities which appear to match the flow pattern of the data vectors. The best model is selected using an error metric.

Two concepts to identify the singular flow are examined. First, a least squares approach is used to identify four parameters which fully characterize the singular flow. This approach yields the minimum identification error and generates a fluid flow model that is valid in the domain where measurements were taken. A second approach preserves intrinsic regional flow characteristics, such as average divergence and vorticity. As shown in the experimental results in Section IV-B, a flow model that reproduces these features adequately captures the regional flow and might also provide reasonable estimates of the fluid motion outside the region of existing measurements.

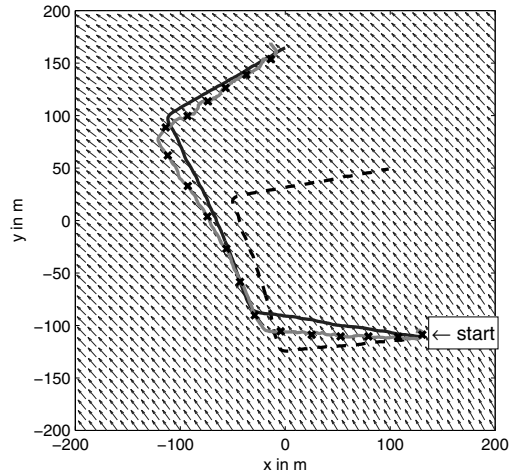


Fig. 7. Dead reckoning: The AUV trajectory is recalculated using the kinematic model (3) with (solid line) and without (dashed line) an ambient flow model. During the field experiment, GPS way points 'x' were collected every 30s along the vehicle's trajectory.

The variety of approaches allows us to adapt the algorithm depending on the identification priority. For example, a bend in a river might suggest a largely rotational singularity while an upwelling event might suggest a largely dilatational singularity. The trade-off between a low RMS error and the capture of regional fluid motion is an issue of current research and will be examined during further field experiments.

REFERENCES

- [1] E. Memin and P. Perez, "Fluid motion recovery by coupling dense and parametric vector fields" *Proceedings of the Seventh IEEE International Conference on Computer Vision* vol.1, 1999, Los Alamitos, CA, USA, pp. 620-5.
- [2] L. Graftieux, M. Michard and N. Grosjean, "Combining PIV, POD and vortex identification algorithms for the study of unsteady turbulent swirling flows" *IOP Publishing, Measurement Science & Technology* vol.12, no.9, Sept. 2001, UK, pp. 1422-9.
- [3] T. Kohlberger, C. Schnorr and E. Memin, "Variational dense motion estimation using a div-curl high-order regularization" *Proceedings of The Seventh International Symposium on Signal Processing and Its Applications* vol.1, 1-4 July 2003, pp. 641-644.
- [4] G. Haller, "Finding finite-time invariant manifolds in two-dimensional velocity fields" *Chaos* 10 2000.
- [5] M. Roth and R. Peikert, "A higher-order method for finding vortex core lines" *Proceedings of Visualization '98 IEEE*. 1998, Piscataway, NJ, USA, pp. 143-50.
- [6] A. Gadre, J.E. Mach, D.J. Stilwell and C.E. Wick, "A prototype miniature autonomous underwater vehicle" *IEEE/RSJ International Conference of Robotics and Automation*.
- [7] K. Polthier and E. Preuss, "Variational approach to vector field decomposition" *Proceedings of the Joint EUROGRAPHICS and IEEE TCVG Symposium on Visualization* Springer-Verlag, 2000, Wien, Austria, pp. 147-155.
- [8] J.K. Knauss, *Introduction to Physical Oceanography* Prentice-Hall, 1978, pp. 111-135.
- [9] H.K. Khalil, *Nonlinear Systems* Prentice Hall, 2nd edition, 1996, pp. 97-113.
- [10] K. Karamcheti, *Principles of Ideal-Fluid Aerodynamics* Krieger Publishing Company, Reprint Edition, 1980.
- [11] A. Gadre and D.J. Stilwell, "Underwater Navigation In the Presence of Unknown Currents Based On Range Measurements From a Single Location" *Proceedings of The American Control Conference* 2005, Portland, OR, USA.
- [12] J. Austin and S. Atkinson, "The design and testing of small, low-cost GPS-tracked surface drifters" *Estuarine* 2004.